Systematic study of (α,γ) reactions for stable nickel isotopes

A. Simon, M. Beard, A. Spyrou, S. J. Quinn, B. Bucher, M. Couder, P. A. DeYoung, A. C. Dombos, J. Görres, A. Kontos, A. Long, M. T. Moran, N. Paul, J. Pereira, D. Robertson, K. Smith, E. Stech, R. Talwar, W. P. Tan, and M. Wiescher

Phys. Rev. C **92**, 025806 — Published 24 August 2015

DOI: 10.1103/PhysRevC.92.025806

Systematic study of (α,γ) reactions for stable nickel isotopes

A. Simon,[1,2,*] M. Beard,[1] A. Spyrou,[2,3,4] S. J. Quinn,[2,3,4] B. Bucher,[1] M. Couder,[1] P. A. DeYoung,[5] A. C. Dombos,[2,3,4] J. Görres,[1] A. Kontos,[1,2,4] A. Long,[1] M. T. Moran,[1] N. Paul,[1] J. Pereira,[2] D. Robertson,[1] K. Smith,[1] E. Stech,[1] R. Talwar,[1] W. P. Tan,[1] and M. Wiescher[1]

[1] *Department of Physics and The Joint Institute for Nuclear Astrophysics, University of Notre Dame, Notre Dame, Indiana 46556, USA*
[2] *National Superconducting Cyclotron Laboratory, Michigan State University, East Lansing, Michigan 48824, USA*
[3] *Department of Physics & Astronomy, Michigan State University, East Lansing, Michigan 48824, USA*
[4] *Joint Institute for Nuclear Astrophysics, Michigan State University, East Lansing, Michigan 48824, USA*
[5] *Department of Physics, Hope College, Holland, Michigan 49423, USA*

A systematic measurement of the (α,γ) reaction for all the stable nickel isotopes has been performed using the γ-summing technique. For two of the isotopes, ^{60}Ni and ^{61}Ni, the α-capture cross sections have been experimentally measured for the first time. For ^{58,62,64}Ni, the current measurement is in excellent agreement with earlier results found in the literature, and additionally extends the energy range of the measured cross sections up to 8.7 MeV. The data provided a tool for testing the cross section predictions of Hauser-Feshbach calculations. The experimental results were compared to the cross sections calculated with the TALYS 1.6 code and commonly used databases: NON-SMOKER and BRUSLIB. For each of the investigated isotopes a combination of input parameter for Talys was identified that best reproduces the experimental data and recommended reaction rate has been calculated. Additionally, a set of inputs for Hauser-Feshbach calculations was given that, simultaneously for all the isotopes under consideration, reproduces the experimental data within the experimental uncertainties.

PACS numbers: 25.40.Lw,24.60.Dr,26.30.Ef

I. INTRODUCTION

The complete description of any stellar nucleosynthesis process requires knowledge of the stellar environment in which the process occurs, as well as information regarding nuclear properties. The nuclear input includes, but is not limited to, reaction rates for all the reactions involved in the process. The nuclear reaction pattern, in particular for explosive processes involving heavy nuclei such as r- [1, 2], rp- [3, 4], νp- [5–7] and p-processes [8–10], includes reactions on very short-lived isotopes. Currently, it is impossible to measure the cross sections for all of the required reactions, especially for nuclei far from stability. As a result, the vast majority of the required reaction rates are based on theoretical models.

For reactions where the level densities are sufficiently high, such that the resonance spacing is small and the resonances overlap, the reaction can be thought of in terms of averaged quantities, In such cases, the reaction cross sections are usually determined by the statistical Hauser-Feshbach (HF) model [11, 12]. However there are limitations to the statistical model approach. For α-capture reactions in particular, the model fails to reproduce the cross sections in the few cases where reactions have been measured experimentally. Discrepancies between the experimental data and model calculations can be substantial [13]. Because statistical model predictions are an integral part of modeling nucleosynthesis processes, it is crucial to quantify, constrain and limit the uncertainties associated with theoretical inputs to improve the predictions of elemental abundances.

To perform a statistical model calculation a number of nuclear physics inputs are required, including deformations, masses, and level data, as well as models to describe level density, γ-strength functions and particle-nucleus optical model potentials. The results of Hauser-Feshbach calculations are sensitive to the details of these inputs. It is usually the case that codes which calculate statistical model cross sections are designed to allow a user to choose between different options for nuclear input models, e.g. level density, γ-strength function and optical potential. As a result a single code package can yield a range of cross section results, depending on the various model combinations selected by the user.

In this work a systematic measurement of the α-capture cross sections for all the stable Ni isotopes was performed using the same experimental γ-summing technique. The results, combined with previous experimental data found in the literature provide an excellent opportunity for testing the Hauser-Feshbach calculations over a wide range of isotopes at Z=28. Nickel isotopes were chosen for this work, as they provide a wide range of stable isotopes to study, while shell-closure ensures a spherical nucleus for which deformation effects, that are difficult to consider in statistical models, are minimized.

The calculations for the current work have been performed using the TALYS 1.6 [14] nuclear reaction code, which is available under GNU General Public License [15]. The experimental Ni(α,γ)Zn data has also been compared to cross section calculations obtained from the

* anna.simon@nd.edu

TABLE I. Properties of the nickel targets utilized during the experiment.

Isotope	Enrichment [%]	Thickness [mg/cm^2]	(α,γ) Q-value [MeV]
^{58}Ni	95(5)	0.943(44)	3.3686(10)
^{60}Ni	95(5)	0.676(90)	3.9564(2)
^{61}Ni	95(5)	0.517(67)	4.1156(1)
^{62}Ni	95(5)	1.66(20)	4.5782(1)
^{64}Ni	40(5)	0.270(14)	5.3328(1)

code package NON-SMOKER [16, 17], and to the specific TALYS nuclear input combinations required to generate the rates provided by the BRUSLIB library [18].

The paper is organized as follows. In Section II the experimental procedure utilized for this work, as well as the results and comparison to previous measurements found in the literature, are presented. The details of the theoretical calculations are summarized in Sec. III. The comparison of the nuclear input model cross section combinations to experimental data, as well as the NON-SMOKER and BRUSLIB databases, are given in Sec. III D. Also provided in Sec. III D are the recommended reaction rates for each target, obtained from the nuclear input model which best describes the experimental data. Finally, conclusions are given in Sec. IV.

II. EXPERIMENTAL PROCEDURE

The experiment was carried out at the University of Notre Dame utilizing an α beam from the 11-MV-tandem-(FN)-Pelletron accelerator. Five isotopically enriched targets of all the stable nickel isotopes ($A = 58, 60, 61, 62, 64$) were used during the experiment. The thickness of each target was determined via the Rutherford Backscattering (RBS) technique, performed at Hope College Ion Beam Analysis Laboratory [19]. The details of the target properties are listed in Table I.

Each of the targets was irradiated with an α beam in the energy range of 5-9 MeV, in 200-500 keV steps. Due to the target thickness typical energy loss of the α beam was of the order of 0.1-0.4 MeV. In Table II the effective reaction energy at the center of the target is given. For each beam energy, the beam current in the range of 4-60 enA was used to maximize the count rate without compromising the live time or increasing the pile-up effects. The beam current was constantly monitored during the experiment using a Faraday cup at the end of the beam line. For a given beam energy the measurements took from a few minutes to an hour, depending on the reaction cross section. The collected data was constantly monitored online to ensure that the number of events in the spectra was sufficient for the analysis.

The γ-rays following the interaction in the target were

TABLE II. (α,γ) reaction cross sections obtained within this work for all the stable Ni isotopes.

E^{eff}_{CM} [MeV]	σ [μb]	E^{eff}_{CM} [MeV]	σ [μb]
	^{58}Ni		
4.988	3.13(44)	6.673	34.0(6.1)
5.171	4.70(60)	7.051	52.4(7.1)
5.360	6.7(1.0)	7.428	66.9(9.7)
5.548	9.6(1.3)	7.805	93(15)
5.922	15.3(2.4)	8.277	139(22)
6.298	22.2(3.5)	8.749	159(25)
	^{60}Ni		
5.016	11.0(1.3)	6.157	127(19)
5.207	18.8 (2.8)	6.347	168(21)
5.398	29.8 (3.8)	6.537	224(27)
5.588	48.8(7.3)	6.725	282(45)
5.777	71.5 (8.8)	6.915	364(49)
5.967	95(10)		
	^{61}Ni		
5.056	2.22(36)	6.384	39.9(4.9)
5.246	3.40(46)	6.573	49.0(7.3)
5.437	5.75(95)	6.761	65.3(8.2)
5.626	11.0(1.4)	6.761	66.2(8.4)
5.815	18.4(2.2)	6.95 0	83(13)
6.004	25.3(4.1)	7.423	135(22)
6.194	33.5(4.4)		
	^{62}Ni		
5.325	55.1(6.0)	6.39	466(58)
5.81	206(24)	6.774	280(41)
6.003	317(51)	7.256	348(54)
6.197	421(57)		
	^{64}Ni		
4.498	2.08(27)	6.496	10.3(1.3)
4.689	5.86(84)	6.969	27.1(3.2)
5.069	2.56(37)	7.443	55.9(6.6)
5.547	1.37(32)	7.917	80.0(8.6)
6.022	3.76(57)	8.39	129(14)

detected with a γ-summing detector, SuN [20], developed at the National Superconducting Cyclotron Laboratory, Michigan State University. SuN is a NaI(Tl) cylinder, 16 in. in diameter and 16 in. in length divided into eight optically isolated segments. The volume of the detector allows for total absorption of all the γ-rays emitted during the reaction. The resulting spectrum contains a single peak, the so-called "sum-peak", at the energy corresponding to the energy difference between the initial and final state of the populated nucleus. Alternatively, the energy of the sum-peak can be expressed as:

$$E_\Sigma = E_{cm} + Q, \quad (1)$$

where E_{cm} is the projectile energy in the center-of-mass frame of reference and Q is the reaction Q-value. Exam-

ples of spectra obtained for each of the targets for the beam energy of 7.0 MeV are shown in Fig. 1. For each of the targets a sum-peak is visible at an energy equal to $E_{cm} + Q$.

The background to the left of the sum peak in all the examples is due to an incomplete summation of the γ-ray energies in the detector and beam scattering off the Ta backing. A thorough discussion of the background contribution to the sum peak in this experiment is given in [21]. If there was no backing, the only source of real background in the sum peak area were cosmic rays. Based on this information, one has to make a choice for how to analyze the sum peak in a consistent way for all experiments. The safest approach was a linear background defined at the 3σ limit from the centroid of the sum peak (similar to what was used in [24]). This analysis procedure was used for efficiency calibration measurements with radioactive sources and with ^{27}Al(p,γ)^{28}Si resonances [20], and is consistent with the calibration of the setup.

For ^{61}Ni, additional structure is present in the spectrum around 9.3 MeV. This is due to the neutrons originating from the (α,n) channel that are detected in the SuN's crystals. Details of the technique and experimental procedures are described in [20] and briefly discussed below.

For each of the beam energy steps, the sum-peak was fitted with a sum of a Gaussian and linear background to determine the width (σ) of the peak, as shown in Fig. 1. After subtraction of the background fit, the sum-peak was integrated in the region ($E_\Sigma - 3\sigma$,$E_\Sigma + 3\sigma$) to obtain the number of events N_Σ. The sum-peaks originating from the other isotopes present in the analyzed targets were well separated from the sum-peak of interest due to the differences in the reaction Q-value. Only in the case of ^{60}Ni and ^{61}Ni is the difference in Q-value less than the width of the integral window. However, due to the high enrichment of both targets, the estimated contribution to the sum-peak from the impurity is less than 1%. In the case of ^{64}Ni the enrichment was the lowest of all targets used (40(5)%), however the sum-peak was well separated from the contributions of the impurities due to its significantly higher reaction Q-value.

The average γ-multiplicity $\langle M \rangle$ for each beam energy was determined from the average number of detector segments that registered a signal during a given event, the so-called "hit pattern". Then, the detection efficiency ϵ_Σ was determined for each pair of E_Σ and $\langle M \rangle$ based on the Geant4 simulations described in [20].

The reaction cross section was calculated from:

$$\sigma = \frac{N_\Sigma}{N_\alpha n_t \epsilon_\Sigma}, \qquad (2)$$

where N_α is the total number of beam particles, and n_t is the areal target density.

For each of the targets the measurements were carried out in a beam energy range as wide as possible, to provide a wide range of cross section data. The lower limit of the energy range was defined by the lowest reaction cross section that could be measured for a given system, i.e. the case where the sum-peak count rate was comparable to the count rate for the background in the same range of the γ-ray spectrum. The higher end was limited by the intensity of the neutrons emitted from the (α,n) channel that rapidly increases with the beam energy after the threshold is reached. The measured cross sections for (α,γ) reactions for each of the targets are shown as solid black circles in Figures 2-6 and are listed in Table II.

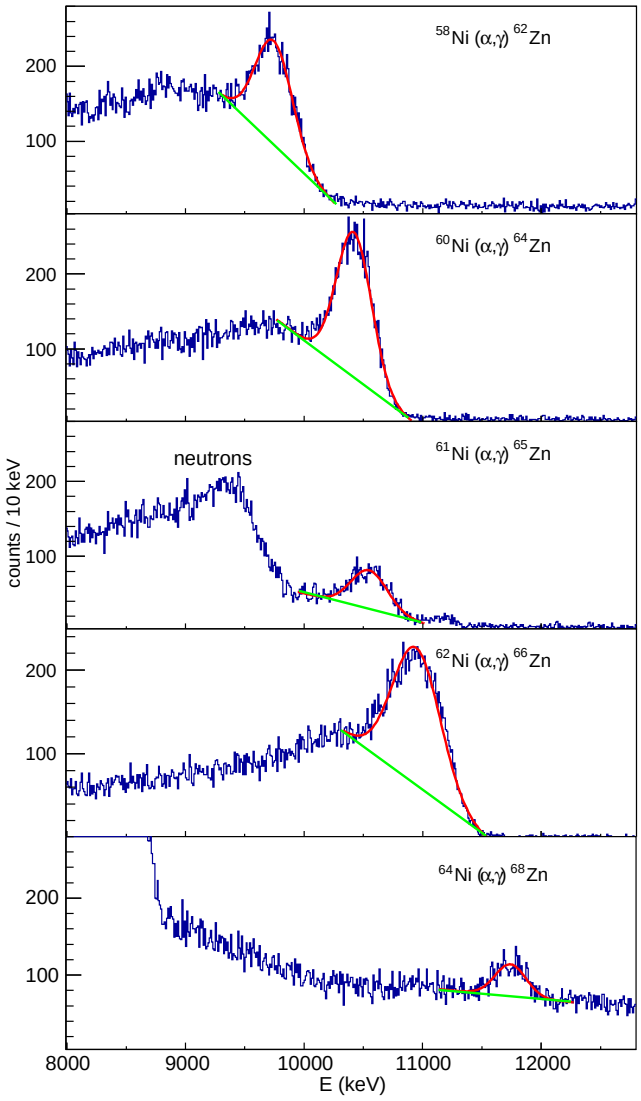

FIG. 1. *(color online)* Sample histograms of the sum peaks obtained for 7 MeV α beam for each of the targets. The shift of the position of the peaks due to differences in the reaction Q-value is clearly visible. For each sum-peak the fitted combination of peak and background is shown (red) and the background under the sum-peak is denoted in green. For ^{61}Ni target additional structure resulting from the neutron from the (α,n) channel is also present.

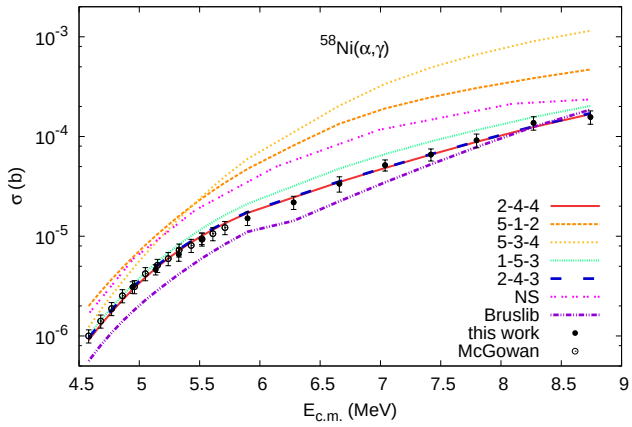

FIG. 2. *(color online)* ^{58}Ni(α,γ)^{62}Zn cross sections obtained in this work (solid circles), and data found in the literature [22] (open symbols). The TALYS 1.6 calculation for model parameter combination which gives the minimum χ^2 for the ^{58}Ni(α,γ)^{62}Zn data set, 2-4-4, is shown as a solid line. The broken lines correspond to the model parameter combinations which resulted in minimum χ^2 for other analyzed targets and the long-dashed line is the 2-4-3 model that gives the best description to all the targets simultaneously (see Section III for detailed explanation). The double-dotted and dot-dashed lines show the cross sections from the NON-SMOKER and BRUSLIB databases, respectively.

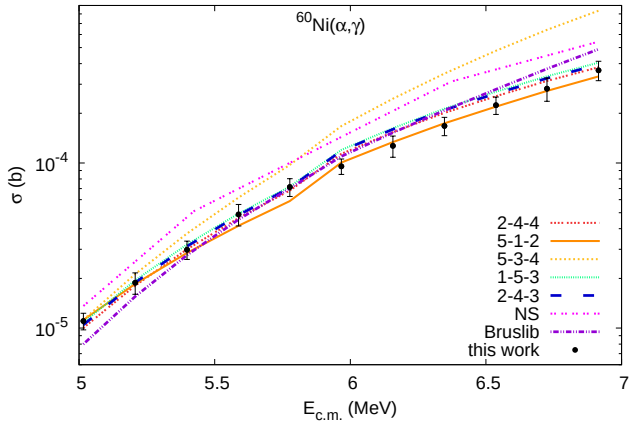

FIG. 3. *(color online)* Same as Fig. 2, but for ^{60}Ni(α,γ)^{64}Zn. The solid line corresponds to the model parameters set 5-1-2.

The uncertainties listed in Table II include both the systematic and statistical uncertainties. The systematic uncertainties in the cross section values are due to the detector efficiency (6.7-16% relative uncertainty), target thickness and enrichment (5%), and beam current (5%). The statistical uncertainty in the number of counts within the sum-peak was in the range of 1.5-7.7%, depending on the number of counts in the sum-peak. The dead time of the measurement was low, typically of the order of 1%.

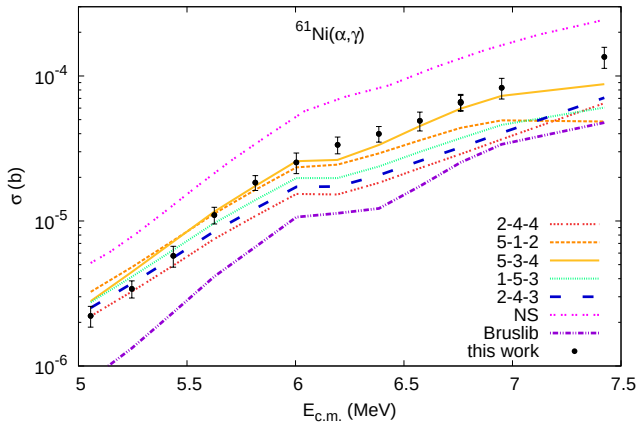

FIG. 4. *(color online)* Same as Fig. 2, but for ^{61}Ni(α,γ)^{65}Zn. The solid line corresponds to the model parameters set 5-3-4.

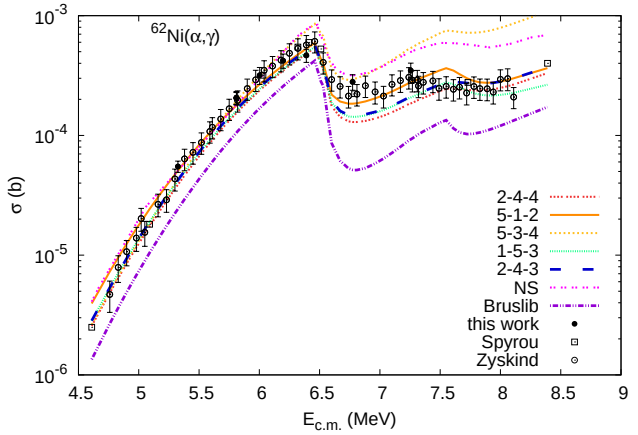

FIG. 5. *(color online)* Same as Fig. 2, but for ^{62}Ni(α,γ)^{66}Zn. The solid line corresponds to the model parameters set 5-1-2. The open symbols correspond to the data from [23, 24].

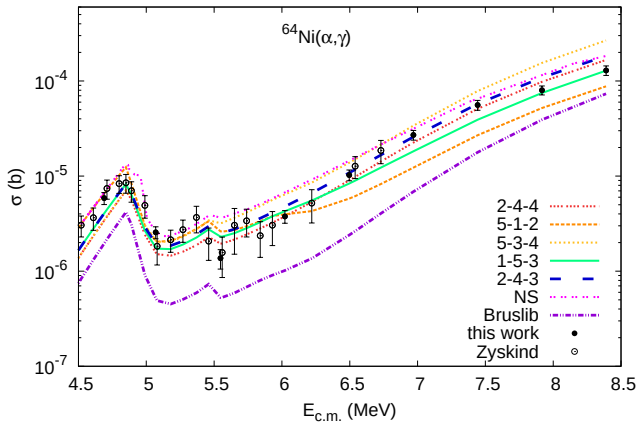

FIG. 6. *(color online)* Same as Fig. 2, but for ^{64}Ni(α,γ)^{68}Zn. The solid line corresponds to the model parameters set 1-5-3. The open symbols denote data from [23].

For three of the targets, ^{58}Ni, ^{62}Ni and ^{64}Ni, previous experimental data exists in the literature. These data are also included in Figs 2, 5 and 6. The ^{58}Ni(α,γ)^{62}Zn cross section was measured by McGowan [22] via coincidence counts of annihilation γ rays from the unstable reaction product, ^{62}Zn. The measurements were conducted in the 4-6 MeV beam energy range. The data reported in the present work is in excellent agreement with that of McGowan and additionally extends the measured energy range up to 8.75 MeV. Detailed discussion of the measurement of the ^{58}Ni(α,γ)^{62}Zn reaction cross section and its impact on stellar nucleosynthesis calculations is given elsewhere [21].

In case of ^{62}Ni, the current measurement covers the same energy range as that investigated by Zyskind et al. [23] and Spyrou et al. [24]. Both measurements were performed using in-beam techniques: Zyskind utilized a small Ge detector at 55° to the beam direction to detect γ-rays feeding the ground state of the reaction product, while Spyrou used a large NaI(Tl) detector for the γ-summing technique. It has to be noted that in the paper Zyskind shows only the statistical errors in the cross-section plots and states in the text that the systematic errors are about 20% of the cross section value. In Fig. 5 the data points from [23] are shown with the total uncertainty that includes both the statistical and systematic uncertainty. All three measurements are in very good agreement with each other throughout the whole beam energy range investigated.

In the same paper, Zyskind and coauthors report a measurement of the ^{64}Ni(α,γ)^{68}Zn cross section, using the same in-beam technique as for ^{62}Ni. Similarly to the ^{62}Ni(α,γ)^{66}Zn, the figures in the original paper show only the statistical errors. Here, in Fig. 6 the data points are given with the total uncertainty, including both statistical and systematic errors. The cross sections reported in the paper agree with the current measurement, but the the new data extends the experimentally covered energy range up to 8.5 MeV.

For two of the targets, ^{60}Ni and ^{61}Ni, the α-capture cross sections have not been measured before.

III. HAUSER-FESHBACH CALCULATIONS

The systematic study of the (α,γ) reactions for all the stable Ni isotopes provides a great tool for testing the HF calculations around Z=28. In order to evaluate the theoretical calculations, the experimental α-capture cross sections for all five nickel isotopes were compared to calculations from the TALYS 1.6 package. There is a very large number of nuclear input model options in the TALYS package that a user can select from to perform a calculation. In order to limit the number of calculations performed, only the level density (LD) model, γ-strength function (gSF), and α optical model potential (aOMP) were investigated. The semi-microscopic JLM optical model [25] was used for neutrons and protons in all of the calculations. The default option for TALYS to normalize the γ-ray transmission coefficients to the average radiative capture width at the neutron threshold for gSF models 1 and 2 (see Sec. III B below) was disabled, so that the γ-strength function was determined directly from the giant dipole resonance parameters. Also disabled was the default option in TALYS to include the effects of pre-equilibrium reactions in the cross sections, however at the low-energies considered in this study contributions from pre-equilibrium reactions are not significant.

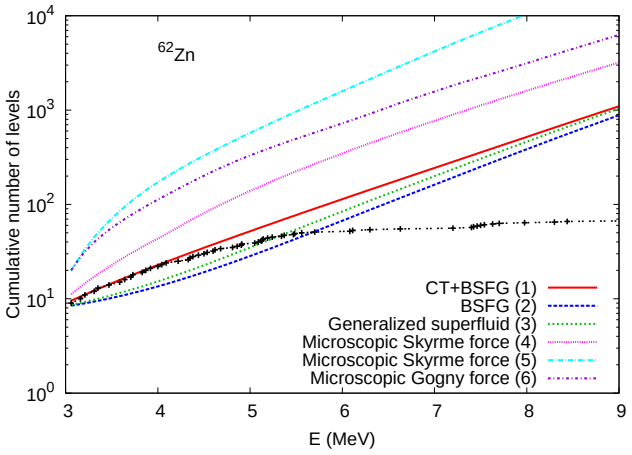

FIG. 7. *(color online)* Cumulative number of levels calculated for ^{62}Zn for the six level density models in the TALYS 1.6 package. The black dotted line refers to the experimentally known levels in ^{62}Zn [26]. At high energies, the experimental data no longer provide a true estimate of the level density. Numbers in brackets refer to the model number in TALYS 1.6.

A. Level density

There are six LD models included in the TALYS Version 1.6 package:

1. Constant temperature matched to the Fermi gas model (CT+BSFG) [27]
2. Back-shifted Fermi gas model (BSFG) [27, 28]
3. Generalized super fluid model [29, 30]
4. Hartree Fock using Skyrme force [31]
5. Hartree-Fock-Bogoliubov (Skyrme force) + combinatorial method [32]
6. Microscopic model, Gogny force [33].

Of these models, the CT+BSFG and BSFG are traditionally the most commonly used in statistical model calculations for nuclear astrophysics. The code NON-SMOKER, used to generate the thermonuclear reaction rate library REACLIB [34] also used the CT+BSFG level

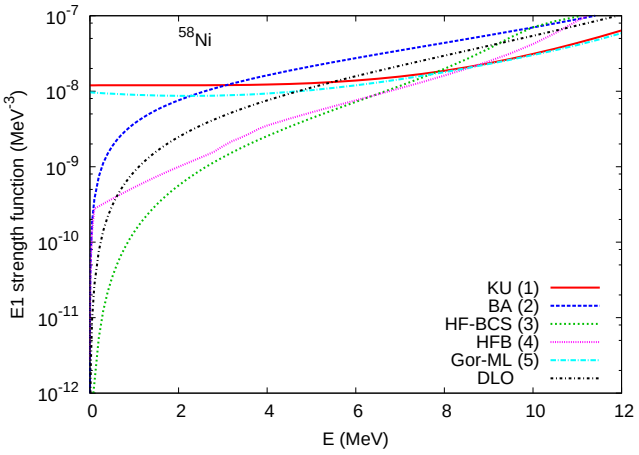

FIG. 8. *(color online)* E1 γ-strength functions for the five models in the TALYS 1.6 package, as well as the model used by the NON-SMOKER code (DLO) [16, 17]. Numbers in brackets refer to the model number in TALYS 1.6.

density description. However it is important to stress that the implementation of the CT+BSFG model in NON-SMOKER differs from that of TALYS in a number of key respects, including the definition of the back-shift, level density and spin-cut off parameters, as well as the temperature and the CT+BSFG matching point energy [35]. When generating the BRUSLIB library [18], TALYS was operated using microscopic model 5 in the above list. For a comparison of the above LD models, the cumulative number of levels as a function of excitation energy for ^{62}Zn has been plotted in Fig. 7. It can be seen that the CT+BSFG model is quite successful at describing the low-energy discreet levels in ^{62}Zn [26], whereas the microscopic models all over-estimate the discreet level density. However, at high energies, the experimental data no longer provides an accurate estimate of the true level density and no conclusion for comparison with the models can be drawn. This result is generally true for all the residual nuclei in this study.

B. E1 γ-strength function

Five E1 gSF models for the giant dipole resonance have been included in the TALYS 1.6 package. These are:

1. Kopecky-Uhl generalized Lorentzian (KU) [36]
2. Brink-Axel Lorentzian (BA) [37, 38]
3. Hartree-Fock BCS (HF-BCS) [26]
4. Hartree-Fock-Bogolyubov (HFB) [26]
5. Modified Lorentzian (Gor-ML) [39].

To aid with visualizing the differences between the gSF models available in the TALYS 1.6 package, the five E1 strength functions are shown for the example case of ^{58}Ni(α,γ)^{62}Zn in Fig. 8. Model 4, the HFB approach from [26], was used to generate the rates in the BRUSLIB library. For comparison, also shown in the plot is the gSF for the double Lorentzian model (DLO), which is used in the NON-SMOKER code.

C. α-optical potential

Five models for the α-optical potential have been included in the TALYS 1.6 package used in the present study:

1. Koning-Delaroche [40]
2. McFadden - Satchler [41]
3. Demetriou et al. given in Table 1 of Ref. [42]
4. Demetriou et al. given in Table 2 of Ref. [42]
5. Demetriou et al. [42], dispersive model.

Models 3 and 4 in the above list are based on the double folding potential with the M3Y effective nucleon-nucleon interaction, but with different parameterizations for the Wood-Saxon description of the imaginary potential. TALYS allows the user to manipulate the double folding potential by modifying both the depth and the shape. For the present study these options were not investigated, so that the aOMP was supplied directly from the model given by Demetriou et al. Model 5 is also based on the same double folding potential, but using the dispersive model. Model 5 was also used in the compilation of the BRUSLIB database, whereas McFadden-Satchler (model 2) was used by the NON-SMOKER code in the generation of the REACLIB database.

D. Results

For each of the Ni targets, calculations of the α-capture cross section were performed utilizing all possible combinations of the level densities, γ-strength functions and α-optical potential models available within TALYS 1.6, listed in Secs. III A – III C.

In order to uniquely distinguish calculations from the LD-gSF-aOMP combinations, a three digit notation was used. The first digit refers to the level density model, 1...6 as listed in Sec III A; the second refers to the γ-strength function, 1...5 as given in Sec III B; and the third corresponds to the α optical model, 1...5 enumerated in Sec. III C. This nomenclature has been used throughout the rest of the paper to describe calculations from the various nuclear input model combinations.

The statistical model calculations were performed at center of mass energies corresponding to the energies for which there was experimental data. Considering all of the available data for a given Ni reaction, a χ^2 minimization was then performed for each calculated cross section

TABLE III. Minimum χ^2 values for model combinations shown in Figs. 2–6. In each case the combinations refer to the 1) level density, 2) γ-strength function and 3) α optical potential model available in the TALYS 1.6 package (See text for details). Additionally, the χ^2 values for several confidence levels α are listed for each target.

Model combination	^{58}Ni	^{60}Ni	^{61}Ni	^{62}Ni	^{64}Ni
			χ^2		
1-5-3	67.36	19.31	81.30	104.84	60.24
2-4-4	6.28	10.39	134.62	138.34	71.66
5-1-2	3477.52	4.08	68.26	75.19	125.61
5-3-4	11720.61	420.78	21.31	1711.34	301.68
2-4-3	7.14	15.78	105.92	93.29	71.82
Accepted discrepancy level			Expected χ^2		
10%	11.7	6.50	6.65	20.5	8.47
20%	46.7	26.0	26.6	82.1	33.9
30%	105	58.5	59.8	185	76.2
50%	292	163	166	513	212

so that the nuclear input model combination that best described the experimental data could be identified.

The nuclear input model combination that yields the minimum χ^2 for each Ni reaction is shown as a solid line in Figs. 2-6 and the χ^2 values are listed in Tab. III. Experimental data considered for the χ^2 minimization are also shown on the plots; solid circles correspond to data measured in the present study, whereas open symbols correspond to data available in the literature.

Using the TALYS code and the input model parameters that best describe the measured cross sections the thermonuclear rate for α-capture was calculated for each of the targets. The obtained reaction rate values are listed in Table IV.

Additionally shown in Figs. 2-6 are the cross sections from two commonly used databases. The first database, REACLIB, provides cross sections calculated using the NON-SMOKER code (NS). The second, BRUSLIB, provides reaction rates rather than cross sections calculated using the TALYS code. In order to obtain the cross sections that could be directly compared with the experimental data, the TALYS calculations were performed using the same set of input parameters as used for BRUSLIB rates [43]. Both the data bases provide cross sections that are significantly different from the experimental values (up to a factor of 2), but are also significantly different from each other. The NS calculations have been performed using the McFadden-Satchler potential [41] and, in general, tend to over-estimate the experimental cross sections. It was pointed out by [42] that the fixed well parameter, energy independent alpha optical model of McFadden results in over-predicted cross sections. On the other hand, the mass and energy dependent dispersive optical potential of [42] tends to result in underprediction for the isotopes considered in the present study. The wide ranging cross sections resulting from these two aOMPs emphasizes the uncertainty and importance of establishing a reliable description of the alpha optical potential.

Along with the nuclear input model combination that results in the minimum χ^2, also plotted in Figs. 2-6 are the model inputs that represent the minimum χ^2 for the other four Ni reactions. The same line color is used for a given model combination through all the figures. For example, plotted as a solid line in Fig. 2 is the model combination 2-4-4, which, as shown in Tab. III, is the LD-gSF-aOMP model combination that gives the minimum χ^2 for ^{58}Ni(α,γ)^{62}Zn reaction. Also plotted in Fig. 2 are the three model combinations that give the minimum χ^2 for the other reactions: 5-1-2 is the minimum χ^2 for ^{60}Ni(α,γ)^{64}Zn and ^{62}Ni(α,γ)^{66}Zn, 5-3-4 is the minimum χ^2 for ^{61}Ni(α,γ)^{65}Zn, and 1-5-3 is the minimum χ^2 for ^{64}Ni(α,γ)^{68}Zn.

It is not very practical to calculate the cross sections for a large range of nuclei using a unique set of input models for each nucleus. For this reason a combination of models that would minimize the discrepancy between the HF predictions and the measured cross sections has been identified. For this purpose χ^2 values were calculated for hypothetical situations when the models reproduce the data within 10%, 20%, 30% and 50%. Typical relative uncertainty for the data discussed in this paper is in the range of 10-30%, thus these limits correspond to the models that, on average, reproduce the data within the experimental uncertainties. The corresponding values of χ^2 for each of the targets are listed in Table III. Then a model that results in the smallest discrepancy from the data simultaneously for all the targets was identified. The chosen model combination, 2-4-3, reproduces the experimental data for ^{58}Ni within 10%, for ^{60}Ni within 20%, ^{62}Ni and ^{64}Ni – within 30% and for ^{61}Ni within 50% of the measured cross section value. The chosen model combination lies within the experimental uncertainty of a vast majority of the the data points for the even-even nuclei For the odd-even ^{61}Ni target the data is underestimated for low energies and

TABLE IV. Recommended reaction rates for (α,γ) reaction for each of the Ni isotopes. Each rate is based on the theoretical model that best describes the data. See text for details.

T [GK]	$N_A\langle\sigma v\rangle$ [cm^{3}mole^{-1}s^{-1}]				
	^{58}Ni	^{60}Ni	^{61}Ni	^{62}Ni	^{64}Ni
0.25	5.22×10^{-42}	2.83×10^{-42}	1.20×10^{-41}	4.11×10^{-42}	5.07×10^{-42}
0.3	1.08×10^{-36}	6.02×10^{-37}	2.54×10^{-36}	8.81×10^{-37}	1.11×10^{-36}
0.4	5.53×10^{-30}	3.23×10^{-30}	1.35×10^{-29}	4.80×10^{-30}	6.51×10^{-30}
0.5	8.81×10^{-26}	5.62×10^{-26}	2.37×10^{-25}	8.53×10^{-26}	1.31×10^{-25}
0.6	9.15×10^{-23}	6.53×10^{-23}	2.68×10^{-22}	1.02×10^{-22}	1.84×10^{-22}
0.7	2.07×10^{-20}	1.66×10^{-20}	6.36×10^{-20}	2.73×10^{-20}	5.41×10^{-20}
0.8	1.77×10^{-18}	1.58×10^{-18}	5.54×10^{-18}	2.72×10^{-18}	5.42×10^{-18}
0.9	7.66×10^{-17}	7.45×10^{-17}	2.39×10^{-16}	1.33×10^{-16}	2.48×10^{-16}
1	1.97×10^{-15}	2.07×10^{-15}	6.06×10^{-15}	3.81×10^{-15}	6.38×10^{-15}
1.5	1.82×10^{-10}	2.63×10^{-10}	4.38×10^{-10}	4.32×10^{-10}	4.50×10^{-10}
2	1.86×10^{-07}	3.45×10^{-07}	3.23×10^{-07}	4.94×10^{-07}	4.03×10^{-07}
2.5	1.82×10^{-05}	4.29×10^{-05}	2.53×10^{-05}	6.14×10^{-05}	3.64×10^{-05}
3	4.60×10^{-04}	1.35×10^{-03}	5.63×10^{-04}	2.04×10^{-03}	8.15×10^{-04}
3.5	5.06×10^{-03}	1.77×10^{-02}	5.73×10^{-03}	2.80×10^{-02}	7.63×10^{-03}
4	3.20×10^{-02}	1.29×10^{-01}	3.47×10^{-02}	2.06×10^{-01}	4.04×10^{-02}
5	4.46×10^{-01}	$2.16\times10^{+00}$	4.57×10^{-01}	$3.19\times10^{+00}$	3.86×10^{-01}
6	$2.56\times10^{+00}$	$1.32\times10^{+01}$	$2.47\times10^{+00}$	$1.59\times10^{+01}$	$1.44\times10^{+00}$
7	$8.55\times10^{+00}$	$4.16\times10^{+01}$	$7.71\times10^{+00}$	$3.76\times10^{+01}$	$3.02\times10^{+00}$
8	$1.99\times10^{+01}$	$8.50\times10^{+01}$	$1.72\times10^{+01}$	$5.82\times10^{+01}$	$4.99\times10^{+00}$
9	$3.72\times10^{+01}$	$1.34\times10^{+02}$	$3.13\times10^{+01}$	$7.41\times10^{+01}$	$7.68\times10^{+00}$
10	$5.96\times10^{+01}$	$1.82\times10^{+02}$	$4.98\times10^{+01}$	$8.78\times10^{+01}$	$1.14\times10^{+01}$

overestimated for high beam energies by at most a factor of two. Such discrepancy is within the acceptable limits of the HF predictions, typically being up to a factor of 3 [17, 44].

It can be clearly seen from Figs 2-6 that one has to be very cautious when choosing the input models for HF calculations as these can result in even an order of magnitude discrepancy between the calculations and measurements. A systematic study of the reactions cross section provide a constrain for the choice of input models in a given range of the chart of nuclides and significantly reduces the discrepancy between the HF prediction and the measured cross sections.

IV. CONCLUSIONS

A systematic measurement of the (α,γ) reaction for all the stable nickel isotopes have been performed using the γ-summing technique. All the measurements were performed using the same technique to avoid possible discrepancies in the result due to various experimental methods used. The data obtained is in an excellent agreement with those found in the literature for ^{58,62,64}Ni and additionally extends the energy range of the measured cross sections up to 8.7 MeV. For two of the isotopes, ^{60}Ni and ^{61}Ni, the α-capture cross sections have been experimentally measured for the first time.

The data was compared with the theoretical prediction of the cross sections from Hauser-Feshbach calculations utilizing the TALYS 1.6 code. A single combination of level density, γ-strength function and optical potential that could reproduce the (α,γ) data for all 5 reactions could not be found, however analysis show that the combination of the level density function using the backshifted Fermi gas model [27, 28], Hartree-Fock-Bogoliubov (HBF) [26] γ-strength function and the α optical potential of Demetriou et al. given in Table 1 of Ref. [42] resulted in the smallest average discrepancy from the data across all the isotopes analyzed. Because this nuclear input model combination reproduced the data to within 30% for all the even-even isotopes and within 50% for ^{61}Ni, it is recommended for the cross section estimations within this mass region when experimental data is not available. Additional experimental data in the Z$\approx$28 region would be valuable to further test the applicability of this combination of Hauser-Feshbach inputs to other nuclei.

The experimental results were also compared with commonly used data bases: NON-SMOKER and BRUSLIB. A significant deviation from the data was found in case of both the data bases, thus, caution is advised when using these predictions for α-capture rates in this mass region.

ACKNOWLEDGMENTS

This work was supported by the National Science Foundation under Grants No.: PHY-1102511 (NSCL), No. PHY-1430152 (JINA-CEE) and PHY-1419765 (NSL).

[1] S. Goriely, Astron. Astrophys. **325**, 414 (1997).
[2] S. Goriely, Phys. Lett. B **436**, 10 (1998).
[3] H. Schatz, A. Aprahamian, J. Görres, M. Wiescher, T. Rauscher, J. Rembges, F.-K. Thielemann, B. Pfeiffer, P. Möller, K.-L. Kratz, H. Herndl, B. Brown, and H. Rebel, Phys. Rep. **294**, 167 (1998).
[4] G. P. A. Berg, Y. Fujita, J. Görres, M. N. Harakeh, K. Hatanaka, A. Long, R. Neveling, F. D. Smit, R. Talwar, A. Tamii, and M. Wiescher, J. Phys.: Conf. Ser. **387**, 012003 (2012).
[5] C. Fröhlich, G. Martinez-Pinedo, M. Liebendörfer, F.-K. Thielemann, E. Bravo, W. R. Hix, K. Laganke, and N. T. Zinner, Phys. Rev. Lett. **96**, 142502 (2006).
[6] J. Pruet, R. D. Hoffman, S. E. Woosley, H.-T. Janka, and R. Buras, Astrophys. J. **644**, 1028 (2006).
[7] S. Wanajo, Astrophys. J. **647**, 1323 (2006).
[8] M. Arnould and S. Goriely, Phys. Rep. **384**, 1 (2003).
[9] T. Rauscher, Proc. of Science PoS(NIC XI) , 059 (2011).
[10] S. E. Woosley and W. M. Howard, Astrophys. J. Suppl. **36**, 285 (1978).
[11] L. Wolfenstein, Phys. Rev. **82**, 690 (1951).
[12] W. Hauser and H. Feshbach, Phys. Rev. **87**, 366 (1952).
[13] G. Gyürky, G. G. Kiss, Z. Elekes, Z. Fülöp, E. Somorjai, A. Palumbo, J. Görres, H. Y. Lee, W. Rapp, M. Wiescher, N. Özkan, R. T. Güray, G. Efe, and T. Rauscher, Phys. Rev. C **74**, 025805 (2006).
[14] A. Koning, S. Hilaire, and M. Duijvestijn, Proc. of the Int. Conf. Nucl. Data for Sci. Tech. - ND2007, May 22 - 27, 2007, Nice , 211 (2008).
[15] GNU General Public License, www.gnu.org/licenses/gpl-2.0.html (2015).
[16] T. Rauscher and F.-K. Thielemann, in *Stellar Evolution, Stellar Explostions and Galactic Chemical Evolution*, edited by A. Mezzacappa (IOP, Brisol, 1998) p. 519.
[17] T. Rauscher and F. K. Thielemann, Atomic Data and Nuclear Data Tables **75**, 1 (2000).
[18] BRUSLIB, http://www.astro.ulb.ac.be/bruslib (2015).
[19] Hope College Ion Beam Analysis Laboratory, www.hope.edu/academic/physics/facilities/accelerator (2015).
[20] A. Simon, S. Quinn, A. Spyrou, A. Battaglia, I. Beskin, A. Best, B. Bucher, M. Couder, P. DeYoung, X. Fang, J. Görres, A. Kontos, Q. Li, S. Liddick, A. Long, S. Lyons, K. Padmanabhan, J. Peace, A. Roberts, D. Robertson, K. Smith, M. Smith, E. Stech, B. Stefanek, W. Tan, X. Tang, and M. Wiescher, Nucl. Instr. Meth. A **703**, 16 (2013).
[21] S. J. Quinn, A. Spyrou, E. Bravo, T. Rauscher, A. Simon, A. Battaglia, M. Bowers, B. Bucher, C. Casarella, M. Couder, P. A. DeYoung, A. C. Dombos, J. Görres, A. Kontos, Q. Li, A. Long, M. Moran, N. Paul, J. Pereira, D. Robertson, K. Smith, M. K. Smith, E. Stech, R. Talwar, W. P. Tan, and M. Wiescher, Phys. Rev. C **89**, 054611 (2014).
[22] F. K. McGowan, P. H. Stelson, and W. G. Smith, Phys. Rev. **133**, 305 (1964).
[23] J. Zyskind, J. Davidson, M. Esat, M. Shapiro, and R. Spear, Nucl. Phys. A **331**, 180 (1979).
[24] A. Spyrou, H. W. Becker, A. Lagoyannis, S. Harissopulos, and C. Rolfs, Phys. Rev. C **76**, 1 (2007).
[25] J.-P. Jeukenne, A. Lejeune, and C. Mahaux, Phys. Rev. C **16**, 80 (1977).
[26] R. Capote, M. Herman, P. Oblozinsky, P. Young, S. Goriely, T. Belgya, A. Ignatyuk, A. Koning, S. Hilaire, V. Plujko, M. Avrigeanu, O. Bersillon, M. Chadwick, T. Fukahori, S. Kailas, J. Kopecky, V. Maslov, G. Reffo, M. Sin, E. Soukhovitskii, P. Talou, H. Yinlu, and G. Zhigang, Nucl. Data Sheets **110**, 3107 (2009).
[27] A. Gilbert and A. Cameron, Can. J. Phys. **43**, 1446 (1965).
[28] W. Dilg, W. Schantl, H. Vonach, and M. Uhl, Nucl. Phys. A **217**, 269 (1973).
[29] A. Ignatyuk, K. Istekov, and G. Smirenkin, Sov. J. Nucl. Phys. **29**, 450 (1979).
[30] A. Ignatyuk, J. Weil, S. Raman, and S. Kahane, Phys. Rev. C **47**, 1504 (1993).
[31] S. Goriely, F. Tondeur, and J. Pearson, Atom. Data Nucl. Data Tables **77**, 311 (2001).
[32] S. Goriely, S. Hilaire, and A. Koning, Phys. Rev. C **78**, 064307 (2008).
[33] S. Hilaire, M. Girod, S. Goriely, and A. Koning, Phys. Rev. C **86**, 064317 (2012).
[34] R. H. Cyburt, A. M. Amthor, R. Ferguson, Z. Meisel, K. Smith, S. Warren, A. Heger, R. D. Hoffman, T. Rauscher, A. Sakharuk, H. Schatz, F. K. Thielemann, and M. Wiescher, Astroph. J. Supp. **189**, 240 (2010).
[35] M. Beard, E. Uberseder, R. Crowter, and M. Wiescher, Phys. Rev. C **90**, 034619 (2014).
[36] J. Kopecky and M. Uhl, Phys. Rev. C **41**, 1941 (1990).
[37] D. Brink, Nucl. Phys. **4**, 215 (1957).
[38] P. Axel, Phys. Rev. **126**, 671 (1962).
[39] S. Goriely, Phys. Rev. Lett. **B436**, 10 (1998).
[40] A. Koning and J. Delaroche, Nucl. Phys. A **713**, 231 (2003).
[41] L. McFadden and G. Satchler, Nucl. Phys. **84**, 177 (1966).
[42] P. Demetriou, C. Grama, and S. Goriely, Nucl. Phys. A **707**, 253 (2002).
[43] S. Goriely, private communication (2015).
[44] J. Holmes, S. Woosley, W. A. Fowler, and B. Zimmerman, Atomic Data and Nuclear Data Tables **18**, 305 (1976).